

Characterization of cellulose nanocrystals extracted from El Diss and El Retma local plants and their dispersion in poly(vinyl alcohol-co-ethylene) matrix in the presence of borax

Polymers and Polymer Composites

1–13

© The Author(s) 2020

Article reuse guidelines:

sagepub.com/journals-permissions

DOI: 10.1177/0967391120910877

journals.sagepub.com/home/ppc



Lilia Benchikh¹ , Abdelhafid Merzouki¹, Yves Grohens²,
Melia Guessoum¹ and Isabelle Pillin²

Abstract

This study aims to investigate the potential of two local fibers, namely El Diss and El Retma, which are abundant in the mountains of North Africa (Sétif, Algeria), to provide cellulose nanocrystals (CNCs). Then, the isolated CNCs from El Diss were used as a reinforcement for a poly(vinyl alcohol-co-ethylene) matrix (EVOH) in the absence and in the presence of borax which was added to improve the interactions between the CNCs and the matrix. The extracted CNCs from both El Diss (CNC_D) and El Retma (CNC_R) were characterized by Zeta-sizer analysis using dynamic light scattering (DLS), Fourier transform infrared spectroscopy (FTIR), thermogravimetric analysis (TGA), and scanning electronic microscopy. Also, untreated EVOH/CNC_D nanocomposites and borax-treated EVOH/CNC_D/BOR have been characterized using FTIR, differential scanning calorimetry (DSC) analyses, and by the study of their water absorption behavior. The DLS analysis provided the transversal length of the particles and showed that the surface of the obtained CNCs is negatively charged due to the presence of sulfated ions. Also, FTIR results confirmed the elimination of extra cellulosic substances, whereas TGA proved that the degradation of CNCs occurs at relatively lower temperatures compared with the neat fibers. The incorporation of borax to EVOH/CNC_D nanocomposites showed its efficiency in improving the interactions at the interface between EVOH and the CNC_D, which significantly affected the material's thermal properties as concluded from DSC results and their water absorption behavior.

Keywords

Bio-based nanocomposites, borax, cellulose nanocrystals, natural fibers, poly(vinyl alcohol-co-ethylene)

Received 20 July 2019; accepted 28 January 2020

Introduction

The development of new materials that combine attractive performances, environmental compatibility, and renewable source actually consists of a potential sustainable alternative to many petroleum-based materials.¹ The rising of the scientific interest in developing bio-based materials and composites using renewable resources is indicated by the steady increase of the number of publications in this topic and the huge advances in improving the properties of biomaterials and biocomposites.²

The use of natural fibers as fillers for polymers continues to receive a privileged interest due to the various improvements concluded on the mechanical properties, among other properties.³ Indeed, the main reasons that have extended the

¹ Laboratoire de Physico-Chimie des Hauts Polymères (LPCHP), Département de Génie des Procédés, Faculté de Technologie, Université Ferhat ABBAS Sétif-1, Algérie

² Institut de Recherche Dupuy de Lôme, UMR CNRS 6027, Université de Bretagne Sud, Lorient, France

Corresponding author:

Lilia Benchikh, Laboratoire de Physico-Chimie des Hauts-Polymères (LPCHP), Département de Génie des Procédés, Faculté de Technologie, Université Ferhat ABBAS Sétif-1, Algérie.

Email: lilia.benchikh@gmail.com

use of vegetable fibers as a principal component of biocomposites are their vast availability, less energy consumption, low-cost production, biodegradability, low density, and high specific strength.⁴

Additionally, the idea of extraction of nanocrystals from natural fibers to produce bio-based nanofillers and promote bio-nanocomposites emerged concomitantly with the development of nanocomposites reinforced with nanominerals.⁵ The aptitude of cellulose to provide nanocrystals (CNC) is conferred by its semicrystalline structure.⁶

Nanocrystals derived from cellulose hold a great promise for an ideal strategy for sustainable development.⁷ They present exceptional characteristics as a high-elastic modulus that is of the order of 100–130 GPa and dependent on the original fiber source as well as a specific surface of several hundred $\text{m}^2 \text{g}^{-1}$ that can be exploited to reinforce polymeric matrices.⁸

CNCs have been extracted from several lignocellulosic sources such as wood, pulps, bagasse, cotton, and recycled paper. Also, numerous approaches for producing CNCs in terms of isolation efficiency and environmental impact have been proposed.⁹ In this context, acid hydrolysis, alkaline and oxidative degradation processes were found to be the most effective routes to extract highly crystalline cellulosic microfibrils. However, the most commonly used process is acid hydrolysis, which involves the removal of amorphous components covering the cellulose fibrils using a strong acid, which in turn results in individual crystallites forming relatively stable suspensions.^{10,11}

The use of CNCs as a reinforcing phase in a wide variety of polymers matrices has been reported.¹² Favier et al.⁵ reported an earlier mechanical enhancement upon the incorporation of tunicate whiskers into a poly(styrene-co-butyl acrylate) latex. This was explained by the formation of a percolating whiskers network in the polymer matrix, in which stress transfer among the whiskers is facilitated by hydrogen bonding. Geng et al.¹³ dispersed CNCs in a poly(vinyl acetate) (PVAc) matrix and found that the in situ polymerized PVAc/CNC composite presented a better dispersion than that showed by the composite produced using mechanical mixing. The investigation of the mechanical and thermomechanical properties revealed that the in situ polymerized nanocomposite with 10 wt% of CNCs exhibited higher strength and storage modulus compared with the mixed composite with the same CNC concentration. Also, Hammiche et al.¹⁴ used CNCs extracted from Alfa to reinforce a poly(vinyl chloride) matrix and obtained noticeable improvements in thermal and thermomechanical performances.

Besides, CNCs are very difficult to disperse in polymers and tend to agglomerate due to their limited stability in aqueous suspension resulting from the high tendency of cellulose nanofibrils to form hydrogen bonds between each other.¹⁵ Although many methods have been conducted to remedy this problem and improve the dispersion of CNCs in polymer matrices, surface chemical modification was found to be the most efficient.¹³

The aim of this work is to explore the possibility and feasibility of efficiently extracting CNCs from two local plants, El Diss and El Retma, thus providing potential candidates for the cost-effective production of CNCs. Afterward, CNCs extracted from El Diss (CNC_D) were incorporated into a poly(vinyl alcohol-co-ethylene) (EVOH) matrix to produce biodegradable materials presenting a better water resistance with respect to composites prepared from natural fibers. To avoid agglomeration of CNC_D and ensure their optimal dispersion, sodium tetraborate was added to induce EVOH cross-linking, which could significantly restrict CNC_D movements and prevent their agglomeration during the nanocomposites processing. Additionally, EVOH cross-linking is expected to notably enhance the material's thermal stability and mediate the high hydrophilic character of the used matrix. After characterizing the microstructure and dimension of the extracted CNCs, the thermal properties and water uptake aptitude of the EVOH/CNC_D composites were also studied.

Experimental

Materials

CNCs were extracted from two plants, El Diss and El Retma, which are abundant in the Sétif (Algeria) region. The reagents used for the extraction process, such as acetone (CH_3COCH_3), sodium hydroxide (NaOH), acetic acid ($\text{CH}_3\text{CO}_2\text{H}$), sodium chlorite (NaClO_2), and sulfuric acid (H_2SO_4), were purchased from Sigma-Aldrich (St. Louis, Missouri, United States). Ethanol ($\text{CH}_3\text{CH}_2\text{OH}$) was purchased from Biochem Chemopharma (Montreal, Quebec, Canada). EVOH used for the preparation of EVOH/CNC_D nanocomposites has the following characteristics: ethylene concentration, 44%; density, 1.140; and melting point, 165°C; EVOH was also provided by Sigma-Aldrich. Dimethylsulfoxide (DMSO) and sodium tetraborate decahydrate (borax; $\text{Na}_2\text{B}_4\text{O}_7 \cdot 10\text{H}_2\text{O}$) used, respectively, for the preparation and treatment of composites were supplied by Sigma-Aldrich.

CNC's extraction from El Diss and El Retma fibers

El Diss and El Retma nanocrystals (CNCs) were prepared by using the method reported earlier by Hammiche et al.¹⁴ This protocol involves three essential steps, which could be described as follows. The first step involves a pretreatment that isolates cellulose by complete or partial elimination of lignin and hemicellulose. A chemical treatment with a strong acid (H_2SO_4) is performed to hydrolyze the amorphous parts in cellulose. At last, the obtained CNCs are dispersed in water to form a stable solution.

Pretreatment. After being washed, dried, and cut, the neat fibers were powdered in a coffee grinder and then sieved to get an average uniform particle size around 100 μm . The powder was treated with acetone/ethanol (38/62; V/V) mixture for 24 h.

Alkali treatment. To remove lignin and hemicellulose, the acetone/ethanol pretreated fibers were subjected to an alkaline treatment carried out five times for 2 h, under magnetic stirring, in a 3% NaOH solution kept in a water bath maintained at a temperature of 80°C. A wash with distilled water was performed after each treatment to remove the residual alkaline solution.

Bleaching of the alkali-treated fibers. The bleaching treatment was performed with a sodium chlorite/glacial acetic acid mixture consisting of equal parts of an acetate buffer (27 g of NaOH and 75 mL of glacial acetic acid and diluted to 1 L of distilled water) and aqueous chlorite (17 g of NaClO_2 in 1 L of distilled water) at 120°C for 2 h under magnetic stirring. This procedure was repeated four times.

Acid hydrolysis. The hydrolysis of the bleached fibers was carried out with a 65% sulfuric acid solution at 50°C in a water bath, for about 1 h, under stirring to remove amorphous regions. Immediately after the acid hydrolysis, the suspension was diluted 10-fold with distilled water to quench the reaction. Successive washings in a centrifuge Universal 16-Hettich (Tuttlingen, Germany) at 5000 rpm for 30 min were then performed. To obtain a stable solution and a better dispersion of CNCs, the CNC solution (concentration: $\sim 0.4\%$ in mass) was treated with ultrasound by a 20 kHz frequency ultrasonic generator for 120 min in water bath using a Vibra-Cell™ Ultrasonic Processor (130 W). Vibra-Cell™ VC 75185, Thermo Fisher Scientific Inc., Waltham, MA, USA.

Preparation of EVOH/CNC formulations

Casting/evaporation method was used to prepare 1% and 3% untreated (EVOH/CNC_D) nanocomposites and borax-treated (EVOH/CNC_D/BOR (borax)) nanocomposite films.

Untreated EVOH/CNC_D nanocomposite films. A mixture of EVOH and DMSO at 10% (W/V) was placed in a water bath at 140°C under continuous stirring for 30 min. In parallel, the CNC_D (0.4%) were sonicated for 2 h, then added to the EVOH solution and stirred until homogenization followed by sonication for 5 min. The mixture was poured into a previously heated dish and then dried in an oven at 60°C until water and DMSO were evaporated. Afterward, the obtained films were immersed in a water bath for 24 h to remove the DMSO traces and finally dried at 60°C.

Treated EVOH/CNC_D nanocomposite films. EVOH/CNC_D/BOR formulations were prepared according to the same procedure described above. For the dispersion of CNC_D, 10 ml of 4% borax solution was added to the polymer under stirring before being poured into a previously heated dish.

Characterization techniques

Characterization of CNCs.

Zeta-sizer analysis: The particle size distribution of CNC samples was estimated by dynamic light scattering (DLS) using a Zeta-sizer nano ZS instrument (Malvern, UK). The dried CNC samples were redispersed in distilled water and then sonicated for few minutes before analysis.

Zeta potential: Surface charges of both the CNCs have been evaluated using zeta potential, which measures the mobility distribution of dispersion of charged particles as they are subjected to an electric field.¹² The analysis was done using DLS (Zeta-sizer nano ZS instrument).

Fourier transform infrared spectroscopy: The chemical composition of raw fibers and dried powders of CNCs was studied using Fourier transform infrared spectroscopy (FTIR). The samples were analyzed with KBr pellets using a Vertex 70v FTIR apparatus (Bruker Corporation, Billerica, MA, USA). FTIR spectra were recorded in absorbance mode, between 4000 cm^{-1} and 400 cm^{-1} and at a resolution of 4 cm^{-1} .

Thermogravimetric analysis: The thermal behavior of the raw fibers and dried CNC samples was studied in a temperature interval ranging between 20°C and 700°C, at a heating rate of 10°C min^{-1} , in nitrogen environment (purge rate details: balance chamber flow rate = 30 $\text{cm}^3 \text{min}^{-1}$ and furnace flow rate = 150 $\text{cm}^3 \text{min}^{-1}$) using a Mettler Toledo thermogravimetric analysis (TGA)/differential scanning calorimetry (DSC) apparatus (Columbus, Ohio, USA).

Scanning electronic microscopy: The morphological characterization of raw fibers and CNC samples was done with a scanning electronic microscope (SEM) using a JSM-6460 apparatus (JEOL Inc., MA, USA).

Characterization methods for EVOH/CNC_D nanocomposites.

FTIR spectroscopy: The molecular interactions between the matrix and CNC_D were investigated by FTIR spectroscopy. The analysis of the EVOH/CNC_D nanocomposite films was performed using a Vertex 70v spectrometer, in absorption mode, in the range between 4000 cm^{-1} and 400 cm^{-1} at a nominal resolution of 4 cm^{-1} .

Differential scanning calorimetry: The thermal characteristics of the nanocomposites before and after the treatment

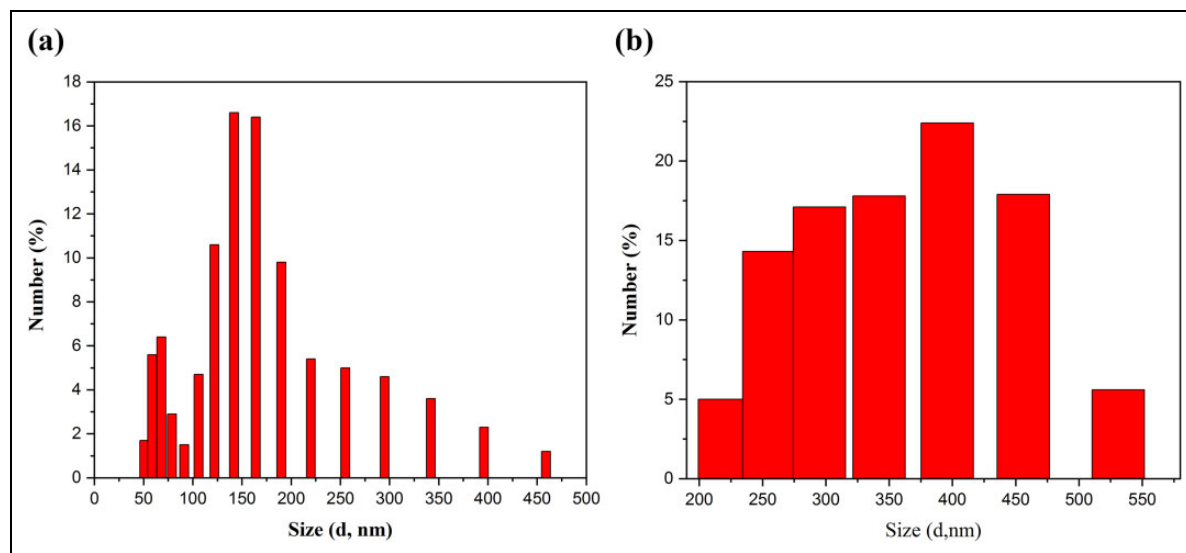


Figure 1. Diameter size distribution of CNCs extracted from (a) El Diss and (b) El Retma fibers. CNCs: cellulose nanocrystals.

were determined using a Mettler Toledo DSC 3 calorimeter under nitrogen flow and at a heating rate of $10^{\circ}\text{C min}^{-1}$. For the analysis, the following heating program has been carried out: heating from 25°C to 200°C , annealing for 2 min at 200°C , cooling from 200° to 0°C , a second annealing for 2 min at 0°C , finally a heating from 0°C to 200°C . From the DSC thermograms giving the variations of the heat flow versus temperature, the glass transition, crystallization, and melting temperatures, respectively, (T_g), (T_c), and (T_m) as well as the crystallization and melting enthalpies, respectively, ΔH_c and ΔH_m , have been determined. The crystallinity degree (χ_c) for each formulation was calculated according to the following equation:

$$\chi_c(\%) = \frac{\Delta H_m}{\Delta H_m^0 \omega} \times 100 \quad (1)$$

ω is the EVOH mass fraction of the composite. The considered melting enthalpy for a 100% crystalline EVOH (ΔH_m^0) is 169.2 J g^{-1} .¹⁶

Water absorption measurements: Films were cut into samples of approximately $1 \times 1 \text{ cm}^2$, which were dried in a vacuum oven at 100°C for 24 h. The initial weights of film samples were evaluated using a Mettler Toledo analytical balance (Columbus, Ohio, USA) with a resolution of 0.0001 g . The samples were then immersed in a closed vessel containing water at room temperature for 72 h. Water uptake measurements were recorded at 24 h intervals and then calculated according to the following equation:

$$\text{Water uptake (\%)} = \frac{m_t - m_0}{m_0} \times 100 \quad (2)$$

where m_t is the mass of the sample at time t and m_0 the mass of the sample before immersion into water.³

Results and discussion

Characterization of CNC_D and CNC_R

CNC sample size characterization. Figure 1(a) and 1(b) presents the size distribution of CNC samples extracted from El Diss and El Retma fibers as determined from DLS, respectively. The figures show most of the particle sizes were between 60 nm and 190 nm and 220 nm and 600 nm for CNC_D and CNC_R , respectively. About 60% of CNC_D reveal a diameter between 70 nm and 170 nm, 20% are less than 100 nm, and 20% are between 220 nm and 460 nm. However, CNC_R nanoparticles show a larger distribution ($>200 \text{ nm}$), where 37% are in the range of 200–300 nm, 60% are between 300 nm and 500 nm, and 6% have a diameter of 530 nm. The discrepancies in particle sizes between the two types of the fibers suggest that El Diss fibers are more susceptible to the performed extraction process, in particular the acid treatment, compared with those derived from El Retma and confirm that particle sizes of CNCs principally depend on their source.¹⁷ The large distribution of both CNC_D and CNC_R may be explained by the eventual existence of nanoparticles aggregates in water, as has been observed by Tang et al.⁷ when extracting CNCs using phosphoric acid. However, Hammiche et al.¹⁴

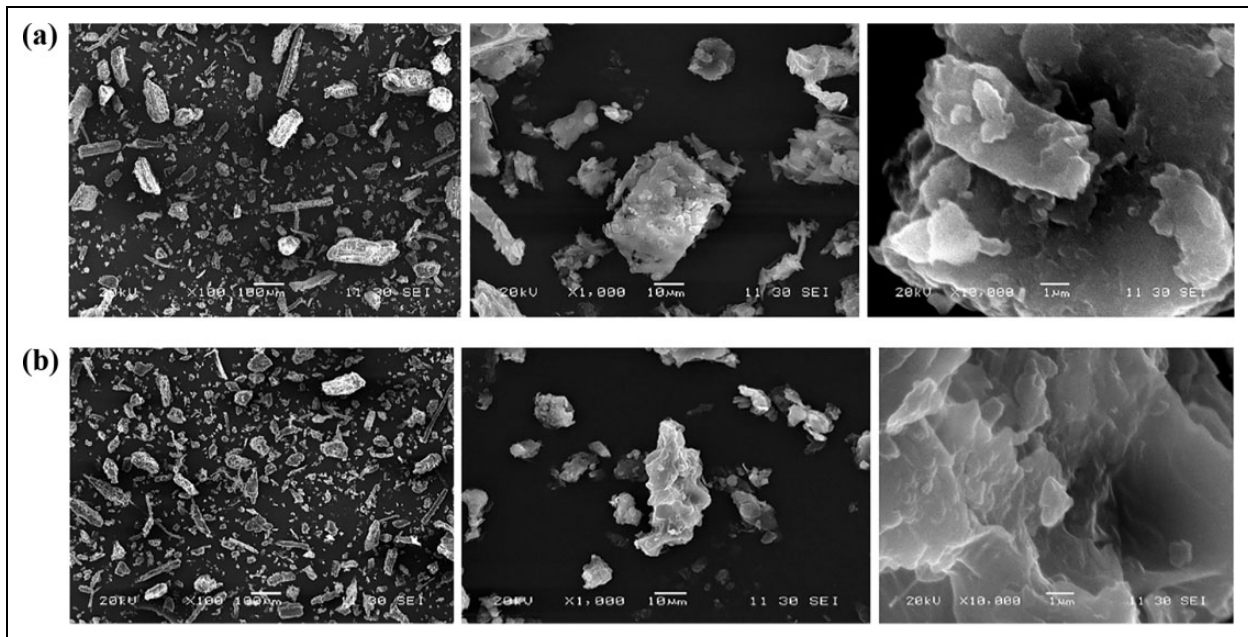


Figure 2. SEM micrographs of (a) El Diss and (b) El Retma raw fibers.
SEM: scanning electronic microscopy.

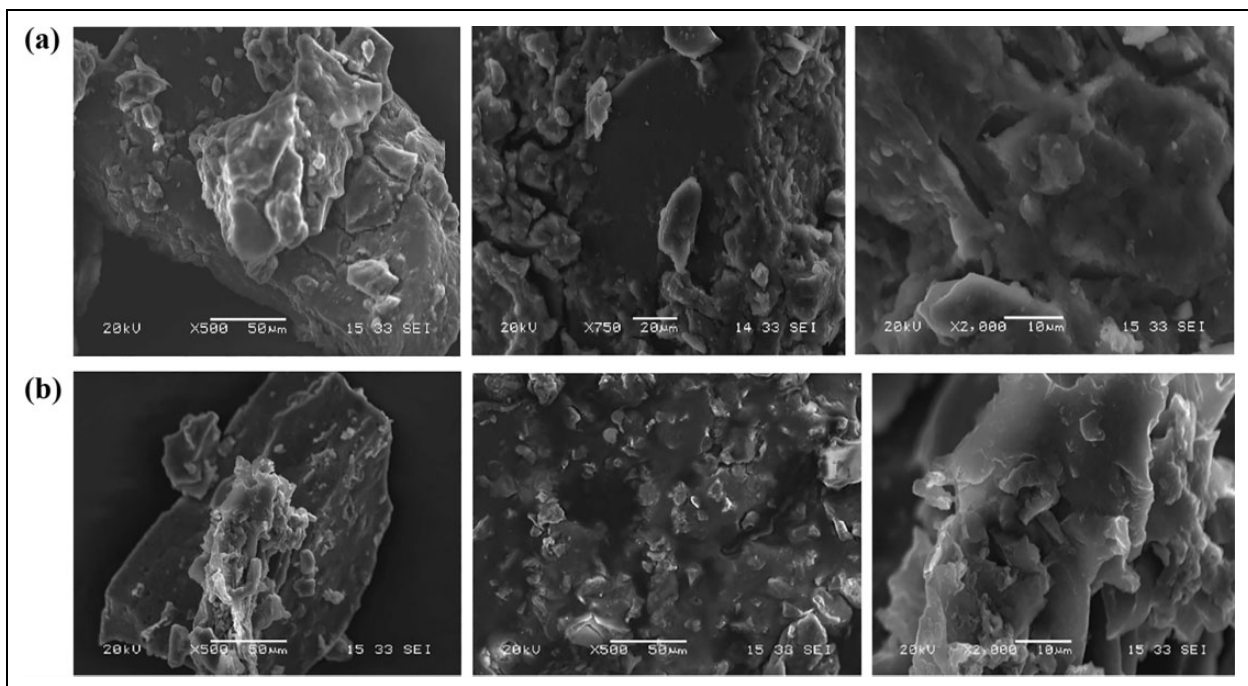


Figure 3. SEM micrographs of dried (a) CNC_D and (b) CNC_R .
SEM: scanning electronic microscopy; CNC: cellulose nanocrystal; CNC_D : CNCs from El Diss; CNC_R : CNCs from El Retma.

suggested that the large size distribution obtained for CNC derived from Alfa fibers is due to their big aspect ratio and that the observed dimensions are influenced by the orientation of CNCs in the solution. Additionally, it is important to point out that the DLS technique probes the particle size based on a spherical model. So when CNCs are not agglomerated into a sphere-like morphology, the evaluated dimensions would still be at least the size of the CNC lengths.

Morphological analysis. Figure 2(a) and 2(b) shows the morphology of El Diss and El Retma raw fibers with different scales, respectively, as determined by SEM. The images reveal that the fibers present different shapes and irregular size distribution. The fiber width varies from 16 μm to 85 μm for El Diss fibers and from 16 μm to 66 μm for El Retma ones. The particles are bonded together due to hydrogen interactions.¹⁸

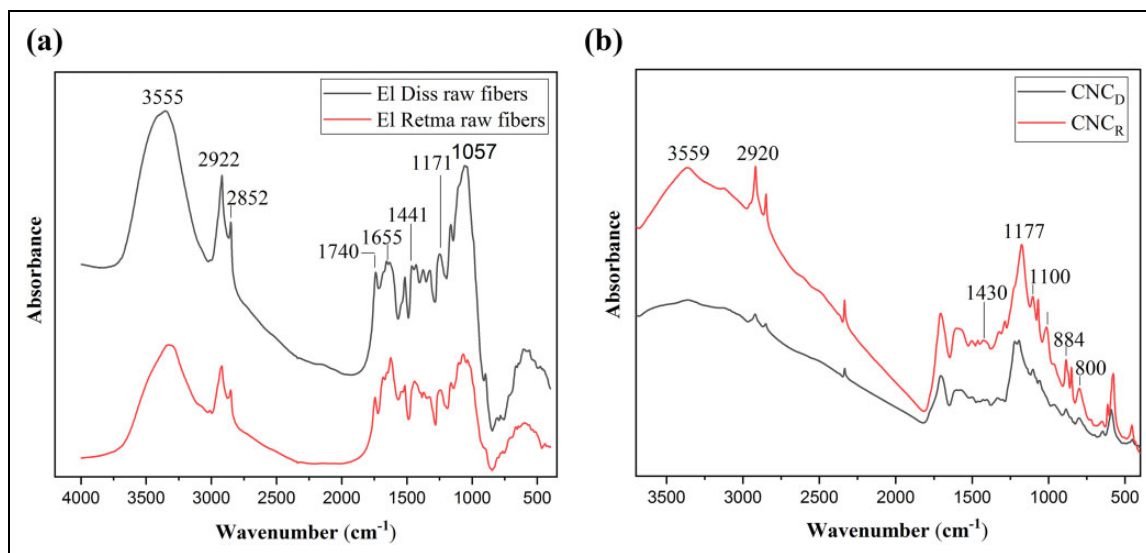


Figure 4. FTIR spectra of (a) El Diss and El Retma raw fibers and (b) CNC_D and CNC_R . FTIR: Fourier transform infrared spectroscopy; CNC_D : CNCs from El Diss; CNC_R : CNCs from El Retma.

SEM images of dry CNC_D and CNC_R are given in Figure 3(a) and 3(b), respectively. The figures exhibit CNC aggregates resulting from the self-assembled fractal structures due to the occurrence of strong hydrogen bonds. These interactions are particularly favored due to the hydroxyl groups existing at the surface of the cellulose fibrils and are highly dependent on the cellulose source and extraction methodology.¹⁰ After CNC drying, the interactions increase, thereby making the rupture of aggregates difficult even after redispersion into water. Such observations agree well with the DLS findings which pointed out the presence of CNCs with variable sizes of CNC_D and CNC_R in the suspensions in water and with the results that have already been reported by many other authors.^{19,20}

Zeta potential. Zeta potential results have shown that both CNC_D and CNC_R manifest negative surface charges of about -39.8 mV and -15 mV, respectively, due to the substitution of the hydroxyl groups present in the cellulosic material by the sulfate ester groups brought by the sulfuric acid used during the hydrolysis step. The presence of these electric charges induces an electrostatic repulsion, which would contribute to the prevention of particle aggregates and thus helps to generate a stable solution of CNC.²¹ In this context, it has been proposed that to obtain colloidal stability, the value of the zeta potential must exceed -30 mV, whereas a value of -15 mV announces the beginning of particle agglomeration.²²

The obtained values show that the zeta potential value of CNC_D is higher than that evaluated for CNC_R . This is an expectable result because CNC_D presents more hydroxyl groups than CNC_R as revealed by their lower particle sizes. This implies that CNC_D presents a larger number of hydroxyl groups that could be esterified by the sulfate ions. On the contrary, CNC_R reveals a limit value for a stable solution. These results fit well with the diameter size distribution which indicated for CNC_D a narrower particle size distribution profile than that obtained for CNC_R . This suggests that during acid hydrolysis, El Diss microfibrils expose more hydroxyl groups to esterification by sulfate ions than El Retma ones. However, El Retma fibrils are less susceptible to esterification probably due to their pronounced tendency to agglomeration. CNCs' characteristics obtained after hydrolysis vary according to the imposed conditions; for example, hydrolysis time and acid-to-pulp weight ratio which affect the particles' dimensions and hydrolysis temperature which could cause dehydration and/or carbonization of the final product.²³ In this case, we could propose that hydrolysis conditions were not enough to induce a sufficient esterification rate for El Retma fibers hydroxyl groups by sulfate ions of the treating agent.

Structure analysis of CNC_D and CNC_R . Figure 4(a) depicts the FTIR spectra of El Diss and El Retma raw fibers. The confirmation of the cellulosic structure of the analyzed samples is provided by the appearance of the main functions that can be enumerated as follows. The large band observed in the range comprised between 3650 cm^{-1} and 3000 cm^{-1} of all the spectra is attributed to the stretching vibrations of hydroxyl groups contained in cellulose and lignin.²⁴ The small bands detected around 2875 cm^{-1} and 1500 cm^{-1} are characteristic of C-H stretching vibrations of lignin. The presence of hemicellulose and pectin is confirmed by the characteristic band between 1730 cm^{-1} and 1745 cm^{-1} attributed to the stretching of carbonyls of the acetyl groups present in these substances. The O-H bending vibration of adsorbed water appears around 1630 cm^{-1} and is due to the hydrophilic character of the cellulosic fibers.^{25,26} The band at 1428 cm^{-1} is attributed to the bending of $-\text{CH}_2$ groups.²⁷ The stretching vibrations of C=C bonds in the aromatic rings of lignin are observed in the range of 1500 – 1600 cm^{-1} .¹⁸ The skeletal vibrations involving C–O stretching appear around 1110 cm^{-1} and 1060 cm^{-1} .²⁸ The band in the region of 1161 cm^{-1} is due to asymmetric stretching of C–O–C of glucose ring in cellulose structure.²⁹

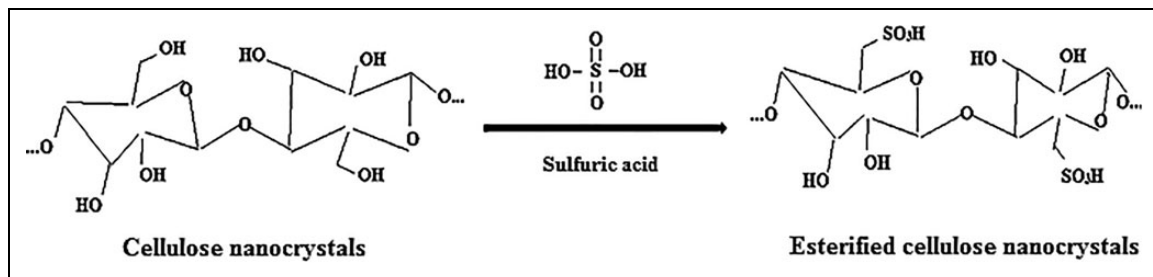


Figure 5. Reaction of cellulose acid hydrolysis with sulfuric acid.

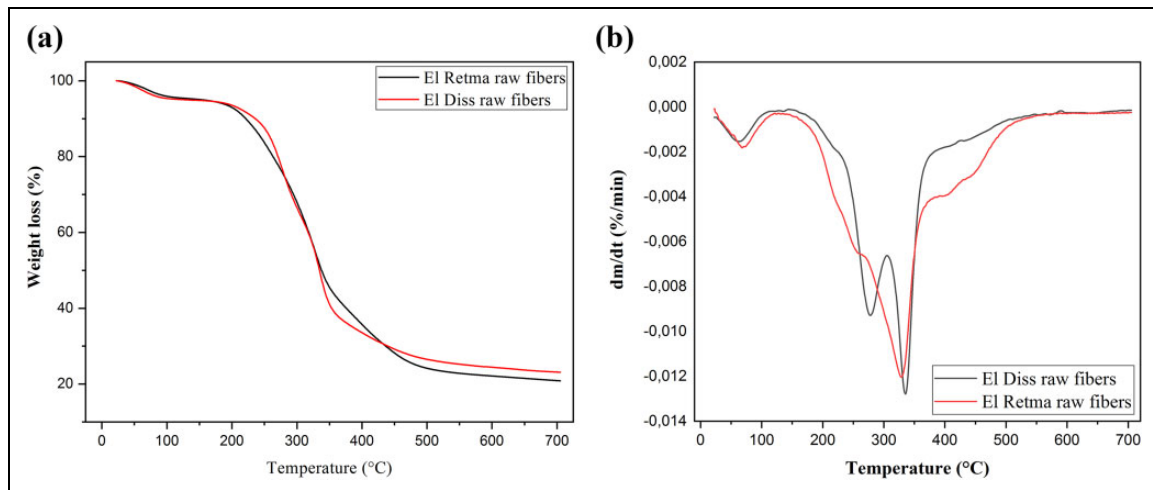


Figure 6. (a) TG and (b) DTG curves of El Diss and El Retma raw fibers. TG: thermogravimetry; DTG: derivative thermogravimetry.

The FTIR spectra of CNC_D and CNC_R are represented in Figure 4(b). The characteristic absorption bands which are displayed by the FTIR spectra of the two samples confirm their cellulosic structure. Also, it is found that acid hydrolysis does not damage the cellulose microstructure of the microfibrils. After hydrolysis treatment, the extraction of CNCs is evidenced by the small band at 888 cm^{-1} attributed to the antisymmetric out-of-plane stretching of glucose ring in cellulose appearing for CNC_R . Additionally, new bands due to the deformation vibrations of CNC groups are detected around 1151 cm^{-1} and 1193 cm^{-1} for CNC_D and at 1173 cm^{-1} for CNC_R . These confirm that the obtained CNCs have the structure of cellulose I.²⁷ In this context, Fortunati et al.²⁷ reported that the weak signal around 800 cm^{-1} confirms the existence of CNCs and their monomeric units after hydrolysis treatment. Also, the presence of signals at 1426 , 1173 , 1099 , and 896 cm^{-1} indicates that the CNCs present primarily the cellulose I microstructure. Moreover, the CNC_D and CNC_R FTIR spectra show that the large band observed between 3000 cm^{-1} and 3700 cm^{-1} and corresponding to $-\text{OH}$ stretching vibration is more prominent compared to raw fibers. This indicates a higher cellulose content and the formation of a large amount of OH groups due to the decomposition of β -1,4-glucosidic linkage.²⁵ Furthermore, the reaction of cellulose with sulfuric acid is supported by the appearance of two new bands around 1200 cm^{-1} which could be assigned to sulfate half-ester groups.¹⁹

On the other hand, it is observed that after treatment with sulfuric acid, the bands assigned to cellulose structure and related to the amount of molecular disorder, particularly those corresponding to $-\text{OH}$ groups stretching vibrations and $-\text{C}-\text{H}-$ stretching vibrations detected at 2920 cm^{-1} become sharper, thus suggesting the increase in the material crystallinity. Similarly, Tang et al.⁷ proposed that the increased absorption intensity may be considered to be related to the increased crystallinity of CNC after hydrolysis and enzymatic treatment. The evaluation of the absorbance ratio at the wavenumbers of 1433 cm^{-1} and 888 cm^{-1} is considered as an adequate route for the comparison of CNC_D and CNC_R crystallinity indexes.³⁰ Their estimation leads to a value of 1.056360 for CNC_R and 1.125287 for CNC_D , which implies that the crystallinity index of the CNC_D is higher than that of CNC_R . Figure 5 shows the reaction pathway of cellulose hydrolysis with sulfuric acid.

Thermal stability assessment by TGA. TGA was performed to compare the raw and acid hydrolyzed cellulose compounds degradation characteristics, as determined from the thermograms reporting the variations of the weight loss (thermogravimetric (TG)) and the derivative of the weight loss versus time (derivative thermogravimetry).

Generally, cellulose degradation processes consist of dehydration, depolymerization, and decomposition of glycosyl units, followed by the formation of a charred residue.³¹

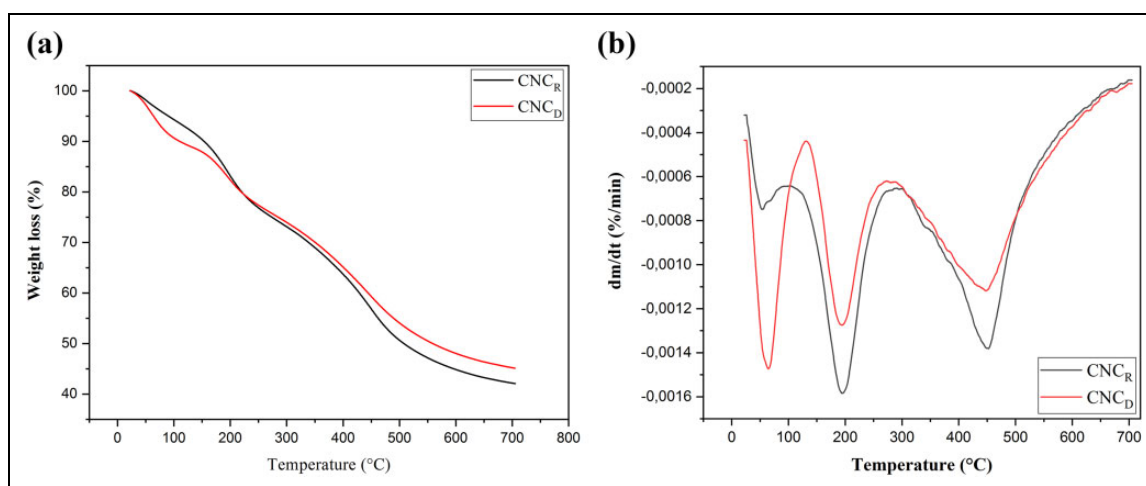


Figure 7. (a) TG and (b) DTG curves of El Diss and El Retma nanocrystals. TG: thermogravimetry; DTG: derivative thermogravimetry.

Figure 6(a) and (b) gives the weight loss and its derivative versus time, respectively, and shows that El Diss and El Retma raw fibers exhibit three main weight loss regions that correspond to different decomposition temperatures for the various components (hemicellulose, lignin, and cellulose) of the two natural fibers.

The initial weight losses were due to the evaporation of chemisorbed water and retained moisture on the surfaces of El Diss and El Retma raw fibers. The main degradation stage, occurring between 220°C and 350°C, corresponds to the thermal decomposition of hemicellulose, pectin, and the cleavage of glycosidic linkages of cellulose.³¹ The peak that appears around 260°C is due to the decomposition of hemicellulose and is more prominent for El Diss raw fiber. The shoulders observed above 350°C are attributed to lignin decomposition. It has been proposed that lignin begins to decompose at a lower temperature than that of cellulose; but at higher temperatures, lignin is more heat resistant than hemicellulose and cellulose because of its low degradation rate.¹⁴

On the other hand, CNC's thermal degradation behavior, displayed in Figure 7(a) and 7(b), presents three main decomposition stages corresponding, respectively, to the evaporation of moisture at low temperature (below 100°C), the primary pyrolysis (150–300°C), and finally the slow charring process of the solid residue (after 300°C).³² Indeed, the first weight loss of CNC_D and CNC_R is detected between 60°C and 140°C and is attributed to the evaporation of absorbed water.³¹ The fraction of evaporated water is more important in the case of El Diss nanocrystals, which corroborates the fact that they contain a higher concentration of –OH groups, as it has been stated from FTIR and Zeta potential results. This also indicates that they are less aggregated and present subsequently a higher specific area than El Retma nanocrystals. The primary pyrolysis of the CNC_D and CNC_R begins around 195°C and is principally assigned to the decomposition of sulfated amorphous regions. This temperature is much lower than the temperature at which the decomposition of native cellulose occurs, i.e. in the range between 250°C and 300°C. The second pyrolysis stage initiates around 450°C and consists of the breakdown of nonsulfated crystals.³³ The decrease in the degradation parameters of CNC_D and CNC_R relatively to those of the raw fibers is due to the released sulfuric acid and the substitution of the hydroxyls by sulfate groups via sulfuric acid hydrolysis. This causes a significant decrease in the activation energy of CNC degradation process.³⁴ In this context, Mao et al.⁹ suggested that the sulfate groups decrease noticeably the thermal stability of natural fiber nanocrystals. They proposed that if these groups are protonated, they are susceptible to catalyzing CNC's decomposition and if they are unprotonated, they can undergo elimination reactions that also decrease CNC's stability.

To explain the difference between the thermal behaviors of CNCs and cellulose fibers, Lu and Hsieh¹⁹ proposed that the promotion of decomposition–gasification processes into CNCs leads to a decrease in their thermal stability. This is induced by the catalyzing effect exerted by the surface groups and the CNC's higher surface area meaning a more important exposed surface to heat phonons which results in their higher thermal conductivity. Hence, the smaller crystallized cellulose chain bundles permit a much more phonon scattering in CNCs than in amorphous chains contained in cellulose, which explains their relatively higher thermal conductivity. Also, Mao et al.⁹ reported that the early decomposition of sulfonated CNCs is promoted by the increased free volume around the areas in the highly sulfated regions, namely the surface and the chain ends.

Characterization of EVOH/CNC_D nanocomposites

Nanocomposites structure analysis. The evolution of the chemical structure for EVOH/CNC_D and EVOH/CNC_D/BOR nanocomposites before and after treatment with borax was investigated by means of FTIR analysis, and the results are reported in Figure 8.

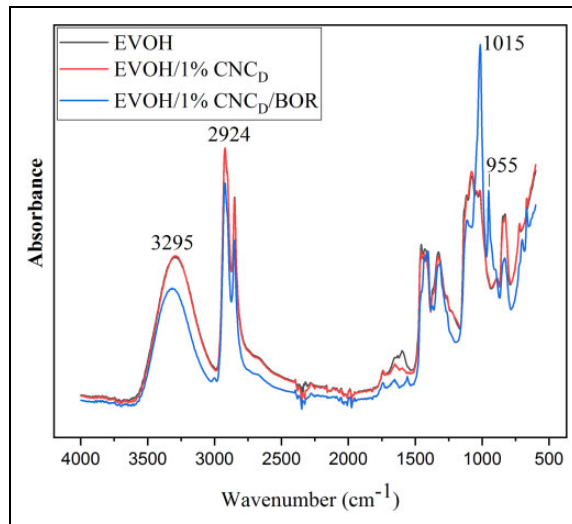


Figure 8. FTIR spectra of untreated and borax-treated EVOH/CNC_D nanocomposites at 1% of CNC_D. FTIR: Fourier transform infrared spectroscopy; EVOH: poly(vinyl alcohol-co-ethylene) matrix; CNC_D: CNCs from El Diss.

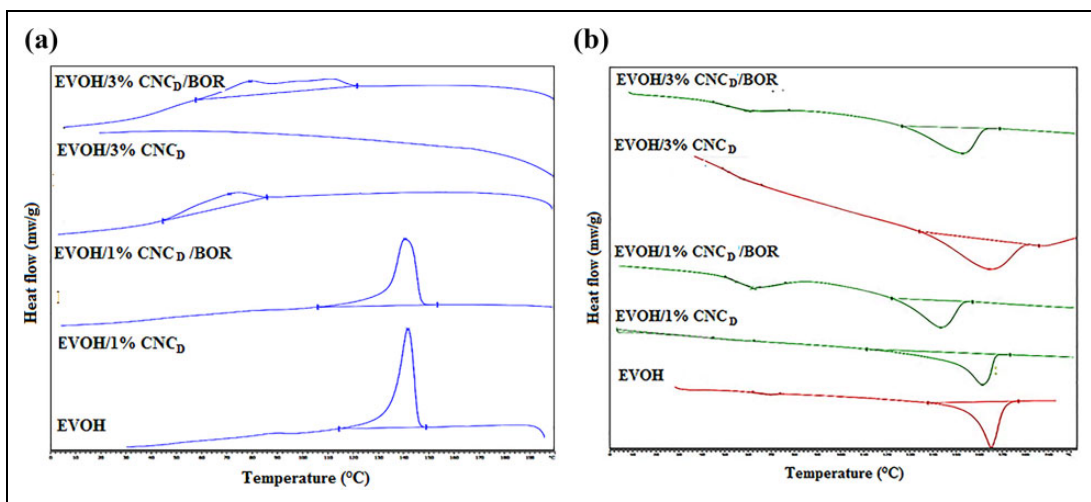


Figure 9. (a) Cooling and (b) second heating DSC thermograms of EVOH/CNC_D and EVOH/CNC_D/BOR nanocomposites. DSC: differential scanning calorimetry; EVOH: poly(vinyl alcohol-co-ethylene) matrix; CNC_D: CNCs from El Diss; BOR: borax.

The chemical structures of the two nanocomposites are similar and the most characteristic cellulose bands overlap with infrared bands of EVOH. Many characteristic bands of common functional groups to both cellulose and EVOH structure appear in the range 3600–3000 cm^{-1} and between 3000 cm^{-1} and 2800 cm^{-1} and are assigned to the hydroxyl groups and alkyl skeleton stretching vibrations, respectively.³⁰ The FTIR spectra of 1% borax-treated EVOH/CNC_D/BOR films show important structural variations because of the appearance of two additional bands at 955 cm^{-1} and 1015 cm^{-1} due to the presence of CNC_D and the decrease in the intensity of the hydroxyl groups. Fortunati et al.³⁵ explained such a decrease in the occurrence of interactions involving the OH groups brought by the CNC nanoparticles and those owing to the EVOH matrix, which is particularly favored in the presence of borax.

Thermal properties of EVOH/CNC_D nanocomposites. DSC measurements have been performed to provide further information about the eventual interactions of CNCs and the EVOH matrix and on the effects of borax. Figure 9(a) and (b) presents, respectively, the cooling and second heating DSC thermograms of neat EVOH and untreated and borax-treated EVOH/CNC_D nanocomposites.

Neat EVOH shows a glass transition temperature around 72°C and a crystallinity that approximates 23%. After the incorporation of CNC_D into the untreated nanocomposites, significant variations are noticed on the whole thermal characteristics of the matrix. The glass transition temperature decreases abruptly by 20°C to attain a value of 52°C. Also, the crystallization exotherm area increases and the maximum of the peak appears at a lower temperature, which is 138°C for the untreated nanocomposite containing 1% of CNC_D. The crystallization exotherm disappears completely for the nanocomposite loaded with 3% of nanocrystals, which suggests that it has totally crystallized during the cooling step

Table 1. Thermal characteristics of EVOH/CNC_D and EVOH/CNC_D/BOR nanocomposites.

Formulations	T_g (°C)	T_c (°C)	ΔH_c (J g ⁻¹)	T_m (°C)	ΔH_m (J g ⁻¹)	χ_c (%)
EVOH	72	142	42	168	39	23
EVOH/1% CNC _D	52	138	51	159	55	32
EVOH/3% CNC _D	52	/	/	158	65	38
EVOH/1% CNC _D /BOR	64	69	8	142	18	11
EVOH/3% CNC _D /BOR	57	74	15	147	22	13

EVOH: poly(vinyl alcohol-co-ethylene) matrix; CNC_D: CNCs from El Diss; BOR: borax.

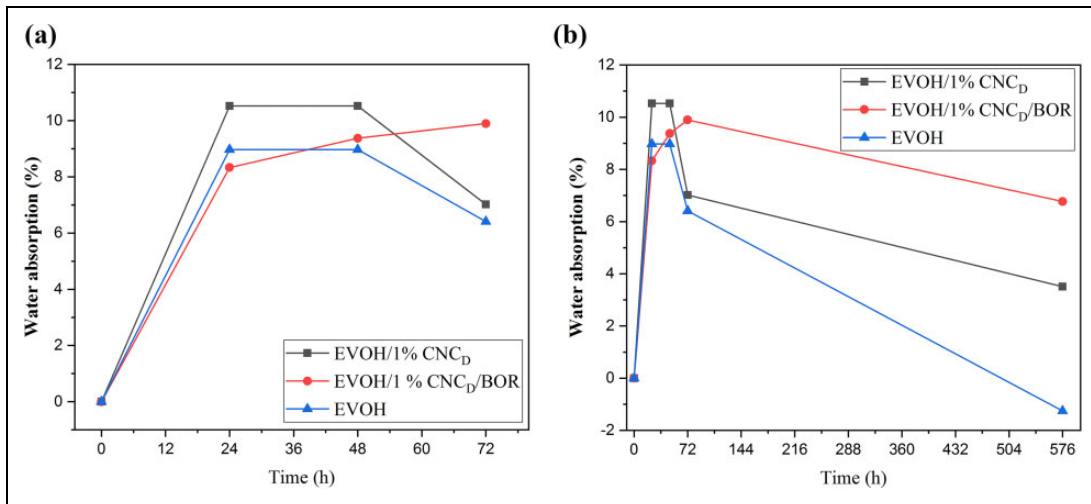


Figure 10. Percentage of water absorption for EVOH/CNC_D and EVOH/CNC_D/BOR at 1% of CNC_D after (a) 72 h and (b) 576 h of water uptake.

EVOH: poly(vinyl alcohol-co-ethylene) matrix; CNC_D: CNCs from El Diss; BOR: borax.

following the processing. As a result of these noticeable changes in the crystallization process, the melting behavior of the untreated nanocomposites shows an important decrease in the melting temperature and an increase in the crystallinity. These results support the fact that the incorporation of CNC induced a substantial plasticizing effect that has contributed to the decrease of the matrix T_g and favored the chains' mobility that has engendered a higher crystallinity and reduced the crystallization temperature. Also, due to this high nucleating effect, the EVOH/CNC_D nanocomposite crystals seem to be less perfect and/or smaller than those formed by the neat matrix, which explains the decrease in the melting temperature. Similar results have been reported when studying PLA/CNC nanocomposites and have been justified by the presence of residual solvent in the films after the casting process.³⁵

EVOH/CNC_D/BOR nanocomposites presented a totally different thermal behavior from that exhibited by the untreated nanocomposites, due especially to EVOH cross-linking and CNC's aggregation. The matrix T_g increases to 64°C and 57°C, relatively to the untreated nanocomposites, for the formulations with 1% and 3% of treated CNC_D nanocomposites, respectively. This means that the plasticizing effect has been attenuated thanks to the interactions established by the borax at the interface between the nanocrystals and the polymer matrix, which limited the chains' mobility.³⁶ The nanocomposite with 3% of CNC presents a lower T_g due to the fact that the higher CNC's concentration into the matrix caused probably more agglomerations and less interactions at the interface. This result fits well with that reported for polyvinyl alcohol (PVA)/sisal nanofibers.³⁷ Additionally, the crystallization exotherms are significantly reduced and their maximum displaced toward lower temperatures implying that a more important supercooling is necessary for the nanocomposites to undergo crystallinity. Due to the disadvantaged crystallization process for the borax-treated CNC_D nanocomposites, the melting enthalpy and the crystallinity values are notably decreased. Also, the EVOH crystals seem to be less perfect and smaller and so they melt at lower temperatures, relatively to those of neat EVOH and untreated EVOH/CNC_D nanocomposites. All these results support the fact that the incorporation of borax induced EVOH cross-linking which increased notably the matrix T_g and hindered its aptitude to crystallization as confirmed from crystallinity values presented in Table 1, which reports the principal thermal characteristics of neat EVOH and EVOH/CNC_D and EVOH/CNC_D/BOR nanocomposites.

Absorption behavior. The behavior of the untreated and borax-treated nanocomposites regarding water absorption is shown in Figure 10. The hydrophilic nature of EVOH allows the absorption of significant amounts of moisture in high-relative humidity conditions. In fact, the polar hydroxyl groups contained in EVOH structure cause its moisture sensitivity because

they are not totally self-associated and are partly isolated in the matrix which interacts with water molecules via hydrogen bonding.³⁸ According to Figure 10(a), EVOH neat matrix presents a mass gain of 8.97%, which is compatible with the results reported earlier by other authors such as Lagaron et al.³⁹ who observed a weight gain of 9.0%, while Aucejo et al.⁴⁰ and Zhang et al.⁴¹ who found values of 13% and 8.4%, respectively, for EVOH films with 32 mol% of ethylene. EVOH water sensitivity was seen to decrease with the increase in ethylene content and degree of crystallinity. The crystallinity increases with vinyl alcohol unit content which restricts chain mobility by intermolecular hydrogen bonding interactions. On the other hand, the increase in the vinyl alcohol unit means increasing hydroxyl groups that will interact with water molecules.³⁸

For EVOH/CNC_D nanocomposites, water absorption occurs simultaneously due to the EVOH matrix through the polar sites present in the polymer, and the cellulose whiskers where the –OH groups of the glucose are a potential site for water uptake and at the interface polymer/CNC_D.⁴² For the untreated sample filled with 1% of CNC_D, only a mass gain of 1% over that of a neat EVOH matrix is noticed. The poor water absorption for EVOH/CNC_D nanocomposite is due to the fact that crystalline cellulose does not absorb significant amounts of water. This also implies that in this case, the water uptake is related predominantly to the EVOH matrix and EVOH/CNC_D interface.⁴³ Also, the weight gain is not significant, thus suggesting a good adhesion between the two components. Additionally, Silvério et al.⁴⁴ reported that the agglomerations of the CNCs dispersed all along the matrix create a barrier against water absorption. Analogously, Saxena⁴⁵ agreed that CNCs form a rigid hydrogen-bonded network, which stops the diffusion of water molecules. However, other studies demonstrated an opposite behavior where water absorption increases with the particles' agglomeration.^{46,47}

In contrast to EVOH/CNC_D nanocomposite, the EVOH/CNC_D/BOR one with 1% of CNC_D shows higher water absorption compared with neat EVOH and its untreated counterpart. This could be interpreted by the fact that after dissolving borax in water, the association of the two compounds generates tetrahydroborate ions B(OH)₄⁻.¹³ These later seem to increase the number of free hydroxyl groups in the composite, which subsequently enhances the water absorption aptitude.

Furthermore, Figure 10(b) shows that the samples' weights decrease when the immersion time is prolonged. This behavior could be explained by the dissolution of PVA contained in the matrix. The weight loss is much more significant for the virgin matrix and decreases after the addition of the CNC_D. This behavior points out the contribution of the interactions between CNC_D and the polymer matrix through their hydroxyl groups in preventing PVA solubilization. Similarly, the material treated with borax exhibited a decrease in weight loss with increasing immersion period, thus corroborating the cross-linking of the EVOH and the improvement of the interactions at the interface CNC_D/matrix.

Conclusion

In the present study, CNCs have been extracted from two abundant local plants which are El Diss and El Retma and then characterized. Afterward, the CNCs obtained from El Diss (CNC_D) have been incorporated in an EVOH matrix. The characterization of CNC_D and CNC_R extracted from El Diss and El Retma, respectively, pointed out, from the analysis of nanoparticles size distribution and Zeta potential measurements, the strong influence of the type of native fibers on the final obtained products. Also, FTIR results evidenced the effectiveness of the performed treatments in the elimination of extra cellulosic materials. This engendered CNCs with a lower thermal stability compared with the corresponding native fibers as deduced from TGA analysis which also confirmed the surface esterification of CNCs.

The treatment with borax, used to improve the dispersion of CNC_D in the EVOH matrix, induced significant variations in the thermal properties of the matrix, thus stating for a better CNCs dispersion and favorable interactions at the interface between the two components. The highly crystalline structure caused a slight increase in the nanocomposites water absorption aptitude that increased in the presence of borax due to the formation of tetrahydroborate ions which introduce more hydroxyl groups into the nanocomposite. It was concluded that by increasing the immersion time, PVA phase dissolution was prevented because of the interactions coupling the matrix to the CNC_D nanoparticles and the cross-linking of EVOH.

Declaration of conflicting interests

The author(s) declared no potential conflicts of interest with respect to the research, authorship, and/or publication of this article.

Funding

The author(s) received no financial support for the research, authorship, and/or publication of this article.

ORCID iD

Lilia Benchikh  <https://orcid.org/0000-0003-4205-8289>

References

1. Neto WPF, Silvério HA, Dantas NO, et al. Extraction and characterization of cellulose nanocrystals from agro-industrial residue—soy hulls. *Ind Crops Prod* 2013; 42: 480–488.
2. Kvien I and Oksman NK. Microscopic examination of cellulose whiskers and their nanocomposites. In: Thomas QH (ed) *Characterization of lignocellulosic materials*. Oxford: Blackwell Publishing Ltd, 2008, pp. 340–356.
3. Dikobe DG and Luyt AS. Effect of filler content and size on the properties of ethylene vinyl acetate copolymer–wood fiber composites. *J Appl Polym Sci* 2006; 103: 3645–3654.
4. Matuana LM, Balatinecz JJ, Sodhi RNS, et al. Surface characterization of esterified cellulosic fibers by XPS and FTIR spectroscopy. *Wood Sci Technol* 2001; 35: 191–201.
5. Favier V, Chanzy H and Cavaille JY. Polymer nanocomposites reinforced by cellulose whiskers. *Macromolecules* 1995; 28: 6365–6367.
6. Philipp HJ, Nelson ML and Ziifle HM. Crystallinity of cellulose fibers as determined by acid hydrolysis. *Text Res J* 1947; 17: 585–596.
7. Tang Y, Shen X, Yanjun JZ, et al. Extraction of cellulose nano-crystals from old corrugated container fiber using phosphoric acid and enzymatic hydrolysis followed by sonication. *J Carbpol* 2015; 125: 360–366.
8. Dufresne A. Cellulose nanomaterial reinforced polymer nanocomposites. *Curr Opin Colloid Interface Sci* 2017; 29: 1–8.
9. Mao J, Abushammala H, Brown N, et al. Comparative assessment of methods for producing cellulose I nanocrystals from cellulosic sources. In: Agarwal UP, Atalla RH and Isogai A (eds) *Nanocelluloses: their preparation, properties, and applications*. ACS Symposium Series; Washington, DC: American Chemical Society, 2017, pp. 19–53.
10. Habibi Y, Lucia LA and Rojas OJ. Chemistry, self-assembly, and applications. *Chem Rev* 2009; 110: 3479–3500.
11. Dufresne A. Polysaccharide nanocrystal reinforced nanocomposites. *Can J Chem* 2008; 86: 484–494.
12. Peng BL, Dhar N, Liu HL, et al. Chemistry and applications of nanocrystalline cellulose and its derivatives: a nanotechnology perspective. *Can J Chem Eng* 2011; 89: 1191–1206.
13. Geng Sh, Haque MdM and Oksman K. Crosslinked poly(vinyl acetate) (PVAc) reinforced with cellulose nanocrystals (CNC): structure and mechanical properties. *Compos Sci Technol* 2016; 126: 35–42.
14. Hammiche D, Boukerrou A, Djidjelli H, et al. Characterization of cellulose nanowhiskers extracted from alfa fiber and the effect of their dispersion methods on nanocomposite Properties. *J Adhes Sci Technol* 2016; 30: 1899–1912.
15. Azizi SMAS, Alloin F, Sanchez JY, et al. Preparation of cellulose whiskers reinforced nanocomposites from an organic medium suspension. *Macromolecules* 2004; 37: 1386–1393.
16. Franzoso F, Vaca-Garcia C, Rouilly A, et al. Extruded versus solvent cast blends of poly(vinyl alcohol-co-ethylene) and biopolymers isolated from municipal biowaste. *J Appl Polym Sci* 2011; 5: 1–10.
17. Börjesson M and Westman G. Crystalline nanocellulose: preparation, modification, and properties. In: Poletto M (ed) *Cellulose—fundamental aspects and current trends*. Rijeka: InTech, Croatia, 2015, pp. 160–191.
18. Li R, Fei J, Cai Y, et al. Cellulose whiskers extracted from mulberry: a novel biomass production. *Carbohydr Polym* 2009; 76: 94–99.
19. Lu P and Hsieh Y. Preparation and properties of cellulose nanocrystals: rods, spheres, and network. *Carbohydr Polym* 2010; 82: 329–336.
20. Ibrahim IK, Hussin SM and Al-Obaidi YM. Extraction of cellulose nano crystalline from cotton by ultrasonic and its morphological and structural characterization. *Int J Mat Chem Phys* 2015; 1: 99–109.
21. Satyamurthy P, Jain P, Balasubramanya RH, et al. Preparation and characterization of cellulose nanowhiskers from cotton fibres by controlled microbial hydrolysis. *Carbohydr Polym* 2010; 83: 122–129.
22. Khalil HPSA, Davoudpour Y, Aprilia NAS, et al. Nanocellulose based polymer nanocomposite: isolation, characterization and applications. In: Thakur VK (ed) *Nanocellulose polymer nanocomposite*. Salem, MA: Scrivener Publishing LLC, 2014, pp. 273–309.
23. Elanthikkal S, Gopalakrishnanapanicker U, Varghese S, et al. Cellulose microfibrils produced from banana plant wastes: isolation and characterization. *Carbohydr Polym* 2010; 80: 852–859.
24. Reddy JP and Rhim J. Isolation and characterization of cellulose nanocrystals from garlic skin. *Mater Lett* 2014; 129: 20–23.
25. Pineda-Pimentel MG, Flores-Ramirez N, Sanchez JCF, et al. Theoretical analysis and FTIR of cellulose nanowhiskers/poly(butylacrylate). *Superficies y Vacío* 2016; 29: 83–86.
26. Zhang X, Wu X, Lu C, et al. Dialysis-free and in situ doping synthesis of polypyrrole@cellulose nanowhiskers nanohybrid for preparation of conductive nanocomposites with enhanced properties. *ACS Sustain Chem Eng* 2015; 3: 675–682.
27. Fortunati E, Puglia D, Mont M, et al. Extraction of cellulose nanocrystals from phormium tenax fibres. *J Polym Environ* 2013; 21: 319–328.
28. Lin Z, Guan Z and Huang Z. New bacterial cellulose/polyaniline nanocomposite film with one conductive side through constrained interfacial polymerization. *Ind Eng Chem Res* 2013; 52: 2869–2874.
29. Kargarzadeh H, Ahmad I, Abdullah I, et al. Effects of hydrolysis conditions on the morphology, crystallinity, and thermal stability of cellulose nanocrystals extracted from kenaf bast fibers. *Cellulose* 2012; 19: 855–866.

30. Martinez-Sanz M, Olsson RT, Lopez-Rubio A, et al. Development of electrospun EVOH fibres reinforced with bacterial cellulose nanowhiskers. Part I: characterization and method optimization. *Cellulose* 2010; 18: 335–347.
31. Chirayil CJ, Mathew L and Thomas S. Review of recent research in nano cellulose preparation from different lignocellulosic fibers. *Rev Adv Mater Sci* 2014; 37: 20–28.
32. Liu DY, Sui GX and Bhattacharyya D. Synthesis and characterization of nanocellulose-based polyaniline conducting films. *Compo Sci Technol* 2014; 99: 31–36.
33. Guoa J, Duc W, Wang S, et al. Cellulose nanocrystals: a layered host candidate for fabricating intercalated nanocomposites. *Carbohydr Polym* 2017; 157: 79–85.
34. Razalli RL, Abdi MM, Tahir PM, et al. Polyaniline-modified nanocellulose prepared from semantan bamboo by chemical polymerization: preparation and characterization. *RSC Adv* 2017; 7: 25191–25198.
35. Fortunati E, Luzi F, Puglia D, et al. Ternary PVA nanocomposites containing cellulose nanocrystals from different sources and silver particles: part II. *Carbohydr Polym* 2013; 97: 837–848.
36. Nigrawal A, Prajapati SCh and Chand N. Mechanical and thermal properties of nano-cellulose obtained from sisal fiber reinforced polyvinyl alcohol (PVA) bio-composites. *J Sci Res Rev* 2012; 1: 40–50.
37. Fortunati E, Rinaldi S, Peltzer M, et al. Nano-biocomposite films with modified cellulose nanocrystals and synthesized silver nanoparticles. *Carbohydr Polym* 2014; 101: 1122–1133.
38. Mokwena KKh and Tang J. Ethylene vinyl alcohol: a review of barrier properties for packaging shelf stable foods. *Crit Rev Food Sci* 2012; 52: 640–650.
39. Lagaron JM, Powell AK and Bonner G. Permeation of water, methanol, fuel and alcohol containing fuels in high barrier ethylene vinyl alcohol copolymer. *Polym Test* 2001; 20: 569–577.
40. Aucejo S, Marco C and Gavara R. Water effect on morphology of EVOH copolymers. *J Appl. Polym Sci* 1999; 74: 1201–1206.
41. Zhang Z, Britt IJ and Tung MA. Water absorption in EVOH films and its influence on glass transition temperature. *J Polym Sci B* 1999; 37: 691–699.
42. Garcia de Rodriguez NL, Thielemans W and Dufresne A. Sisal cellulose whiskers reinforced polyvinyl acetate nanocomposites. *Cellulose* 2006; 13: 261–270.
43. Fortunati E, Puglia D, Luzi F, et al. Binary PVA bio-nanocomposites containing cellulose nanocrystals extracted from different natural sources: part I. *Carbohydr Polym* 2013; 97: 825–836.
44. Silvério HA, Neto WPF and Pasquini D. Effect of incorporating cellulose nanocrystals from corncob on the tensile, thermal and barrier properties of poly(vinyl alcohol) nanocomposites. *J Nanomater* 2013; 2013: 1–9.
45. Saxena A. *Nanocomposites based on nanocellulose whiskers*. PhD Thesis, Georgia Institute of Technology, Atlanta, GA, 2013.
46. Ouna AA and Rhim J. Effect of post-treatments and concentration of cotton linter cellulose nanocrystals on the properties of agar-based nanocomposite films. *Carbohydr Polym* 2015; 134: 20–29.
47. Espino-Pérez E, Bras J, Ducruet V, et al. Influence of chemical surface modification of cellulose nanowhiskers on thermal, mechanical, and barrier properties of poly(lactide) based bionanocomposites. *Eur Polym J* 2013; 135: 255–266.